Submitted to the International Europhysics Conference on High Energy Physics,
HEP97, Jerusalem, Israel, August 1997

DESY 97-095 ISSN 0418-9833
May 1997

Photoproduction of K^0 and Λ at HERA and a Comparison with Deep Inelastic Scattering

H1 Collaboration

Abstract

Inclusive K^0 and Λ photoproduction has been investigated at HERA with the H1 detector at an average photon-proton center of mass energy of 200 GeV in the transverse momentum range $0.5 < p_t < 5$ GeV. The production rates as a function of p_t and center of mass rapidity are compared to those obtained in deep inelastic scattering at $\langle Q^2 \rangle = 23$ GeV^2. A similar comparison is made of the rapidity spectra of charged particles. The rate of strangeness photoproduction is compared with $p\bar{p}$ measurements. The observations are also compared with next-to-leading order QCD calculations and the predictions of a Monte Carlo model.

Abstract 269
Parallel Sessions 2, 3, 4
Plenary Sessions 1, 2, 4

C. Adloff[35], S. Aïd[13], M. Anderson[23], V. Andreev[26], B. Andrieu[29], V. Arkadov[36], C. Arndt[11], I. Ayyaz[30], A. Babaev[25], J. Bähr[36], J. Bán[18], Y. Ban[28], P. Baranov[26], E. Barrelet[30], R. Barschke[11], W. Bartel[11], U. Bassler[30], H.P. Beck[38], M. Beck[14], H.-J. Behrend[11], A. Belousov[26], Ch. Berger[1], G. Bernardi[30], G. Bertrand-Coremans[4], R. Beyer[11], P. Biddulph[23], P. Bispham[23], J.C. Bizot[28], K. Borras[8], F. Botterweck[27], V. Boudry[29], S. Bourov[25], A. Braemer[15], W. Braunschweig[1], V. Brisson[28], W. Brückner[14], P. Bruel[29], D. Bruncko[18], C. Brune[16], R. Buchholz[11], L. Büngener[13], J. Bürger[11], F.W. Büsser[13], A. Buniatian[4], S. Burke[19], M.J. Burton[23], G. Buschhorn[27], D. Calvet[24], A.J. Campbell[11], T. Carli[27], M. Charlet[11], D. Clarke[5], B. Clerbaux[4], S. Cocks[20], J.G. Contreras[8], C. Cormack[20], J.A. Coughlan[5], A. Courau[28], M.-C. Cousinou[24], B.E. Cox[23], G. Cozzika[9], D.G. Cussans[5], J. Cvach[31], S. Dagoret[30], J.B. Dainton[20], W.D. Dau[17], K. Daum[40], M. David[9], C.L. Davis[19,41], A. De Roeck[11], E.A. De Wolf[4], B. Delcourt[28], M. Dirkmann[8], P. Dixon[19], W. Dlugosz[7], C. Dollfus[38], K.T. Donovan[21], J.D. Dowell[3], H.B. Dreis[2], A. Droutskoi[25], J. Ebert[35], T.R. Ebert[20], G. Eckerlin[11], V. Efremenko[25], S. Egli[38], R. Eichler[37], F. Eisele[15], E. Eisenhandler[21], E. Elsen[11], M. Erdmann[15], A.B. Fahr[13], L. Favart[28], A. Fedotov[25], R. Felst[11], J. Feltesse[9], J. Ferencei[18], F. Ferrarotto[33], K. Flamm[11], M. Fleischer[8], M. Flieser[27], G. Flügge[2], A. Fomenko[26], J. Formánek[32], J.M. Foster[23], G. Franke[11], E. Gabathuler[20], K. Gabathuler[34], F. Gaede[27], J. Garvey[3], J. Gayler[11], M. Gebauer[36], R. Gerhards[11], A. Glazov[36], L. Goerlich[6], N. Gogitidze[26], M. Goldberg[30], D. Goldner[8], K. Golec-Biernat[6], B. Gonzalez-Pineiro[30], I. Gorelov[25], C. Grab[37], H. Grässler[2], T. Greenshaw[20], R.K. Griffiths[21], G. Grindhammer[27], A. Gruber[27], C. Gruber[17], T. Hadig[1], D. Haidt[11], L. Hajduk[6], T. Haller[14], M. Hampel[1], W.J. Haynes[5], B. Heinemann[11], G. Heinzelmann[13], R.C.W. Henderson[19], H. Henschel[36], I. Herynek[31], M.F. Hess[27], K. Hewitt[3], K.H. Hiller[36], C.D. Hilton[23], J. Hladký[31], M. Höppner[8], D. Hoffmann[11], T. Holtom[20], R. Horisberger[34], V.L. Hudgson[3], M. Hütte[8], M. Ibbotson[23], Ç. İşsever[8], H. Itterbeck[1], A. Jacholkowska[28], C. Jacobsson[22], M. Jacquet[28], M. Jaffre[28], J. Janoth[16], D.M. Jansen[14], L. Jönsson[22], K. Johannsen[11], D.P. Johnson[4], H. Jung[22], P.I.P. Kalmus[21], M. Kander[11], D. Kant[21], U. Kathage[17], J. Katzy[15], H.H. Kaufmann[36], O. Kaufmann[15], M. Kausch[11], S. Kazarian[11], I.R. Kenyon[3], S. Kermiche[24], C. Keuker[1], C. Kiesling[27], M. Klein[36], C. Kleinwort[11], G. Knies[11], T. Köhler[1], J.H. Köhne[27], H. Kolanoski[39], S.D. Kolya[23], V. Korbel[11], P. Kostka[36], S.K. Kotelnikov[26], T. Krämerkämper[8], M.W. Krasny[6,30], H. Krehbiel[11], D. Krücker[27], A. Küpper[35], H. Küster[22], M. Kuhlen[27], T. Kurča[36], J. Kurzhöfer[8], B. Laforge[9], M.P.J. Landon[21], W. Lange[36], U. Langenegger[37], A. Lebedev[26], F. Lehner[11], V. Lemaitre[11], S. Levonian[29], M. Lindstroem[22], F. Linsel[11], J. Lipinski[11], B. List[11], G. Lobo[28], J.W. Lomas[23], G.C. Lopez[12], V. Lubimov[25], D. Lüke[8,11], L. Lytkin[14], N. Magnussen[35], H. Mahlke-Krüger[11], E. Malinovski[26], R. Maraček[18], P. Marage[4], J. Marks[15], R. Marshall[23], J. Martens[35], G. Martin[13], R. Martin[20], H.-U. Martyn[1], J. Martyniak[6], T. Mavroidis[21], S.J. Maxfield[20], S.J. McMahon[20], A. Mehta[5], K. Meier[16], P. Merkel[11], F. Metlica[14], A. Meyer[11], A. Meyer[13], H. Meyer[35], J. Meyer[11], P.-O. Meyer[2], A. Migliori[29], S. Mikocki[6], D. Milstead[20], J. Moeck[27], F. Moreau[29], J.V. Morris[5], E. Mroczko[6], D. Müller[38], T. Walter[38], K. Müller[11], P. Murín[18], V. Nagovizin[25], R. Nahnhauer[36], B. Naroska[13], Th. Naumann[36], I. Négri[24], P.R. Newman[3], D. Newton[19], H.K. Nguyen[30], T.C. Nicholls[3], F. Niebergall[13], C. Niebuhr[11], Ch. Niedzballa[1], H. Niggli[37], G. Nowak[6], T. Nunnemann[14], M. Nyberg-Werther[22], H. Oberlack[27], J.E. Olsson[11], D. Ozerov[25], P. Palmen[2], E. Panaro[11], A. Panitch[4], C. Pascaud[28], S. Passaggio[37], G.D. Patel[20], H. Pawletta[2], E. Peppel[36], E. Perez[9], J.P. Phillips[20], A. Pieuchot[24], D. Pitzl[37], R. Pöschl[8], G. Pope[7], B. Povh[14], S. Prell[11], K. Rabbertz[1], P. Reimer[31], H. Rick[8], S. Riess[13], E. Rizvi[21], P. Robmann[38], R. Roosen[4], K. Rosenbauer[1], A. Rostovtsev[30], F. Rouse[7], C. Royon[9], K. Rüter[27], S. Rusakov[26], K. Rybicki[6], D.P.C. Sankey[5], P. Schacht[27], S. Schiek[13], S. Schleif[16], P. Schleper[15], W. von Schlippe[21], D. Schmidt[35], G. Schmidt[13], L. Schoeffel[9], A. Schöning[11], V. Schröder[11], E. Schuhmann[27], B. Schwab[15], F. Sefkow[38], A. Semenov[25], V. Shekelyan[11], I. Sheviakov[26], L.N. Shtarkov[26], G. Siegmon[17], U. Siewert[17], Y. Sirois[29], I.O. Skillicorn[10], T. Sloan[19], P. Smirnov[26], M. Smith[20], V. Solochenko[25], Y. Soloviev[26], A. Specka[29], J. Spiekermann[8], S. Spielman[29], H. Spitzer[13], F. Squinabol[28], P. Steffen[11], R. Steinberg[2], J. Steinhart[13], B. Stella[33], A. Stellberger[16], J. Stier[11], J. Stiewe[16], U. Stößlein[36], K. Stolze[36], U. Straumann[15], W. Struczinski[2], J.P. Sutton[3], S. Tapprogge[16], M. Taševský[32], V. Tchernyshov[25], S. Tchetchelnitski[25], J. Theissen[2], G. Thompson[21], P.D. Thompson[3], N. Tobien[11], R. Todenhagen[14], P. Truöl[38], G. Tsipolitis[37],

J. Turnau[6], E. Tzamariudaki[11], P. Uelkes[2], A. Usik[26], S. Valkár[32], A. Valkárová[32], C. Vallée[24], P. Van Esch[4], P. Van Mechelen[4], D. Vandenplas[29], Y. Vazdik[26], P. Verrecchia[9], G. Villet[9], K. Wacker[8], A. Wagener[2], M. Wagener[34], R. Wallny[15], B. Waugh[23], G. Weber[13], M. Weber[16], D. Wegener[8], A. Wegner[27], T. Wengler[15], M. Werner[15], L.R. West[3], S. Wiesand[35], T. Wilksen[11], S. Willard[7], M. Winde[36], G.-G. Winter[11], C. Wittek[13], M. Wobisch[2], H. Wollatz[11], E. Wünsch[11], J. Žáček[32], D. Zarbock[12], Z. Zhang[28], A. Zhokin[25], P. Zini[30], F. Zomer[28], J. Zsembery[9], and M. zurNedden[38]

[1] I. Physikalisches Institut der RWTH, Aachen, Germany[a]
[2] III. Physikalisches Institut der RWTH, Aachen, Germany[a]
[3] School of Physics and Space Research, University of Birmingham, Birmingham, UK[b]
[4] Inter-University Institute for High Energies ULB-VUB, Brussels; Universitaire Instelling Antwerpen, Wilrijk; Belgium[c]
[5] Rutherford Appleton Laboratory, Chilton, Didcot, UK[b]
[6] Institute for Nuclear Physics, Cracow, Poland[d]
[7] Physics Department and IIRPA, University of California, Davis, California, USA[e]
[8] Institut für Physik, Universität Dortmund, Dortmund, Germany[a]
[9] CEA, DSM/DAPNIA, CE-Saclay, Gif-sur-Yvette, France
[10] Department of Physics and Astronomy, University of Glasgow, Glasgow, UK[b]
[11] DESY, Hamburg, Germany[a]
[12] I. Institut für Experimentalphysik, Universität Hamburg, Hamburg, Germany[a]
[13] II. Institut für Experimentalphysik, Universität Hamburg, Hamburg, Germany[a]
[14] Max-Planck-Institut für Kernphysik, Heidelberg, Germany[a]
[15] Physikalisches Institut, Universität Heidelberg, Heidelberg, Germany[a]
[16] Institut für Hochenergiephysik, Universität Heidelberg, Heidelberg, Germany[a]
[17] Institut für Reine und Angewandte Kernphysik, Universität Kiel, Kiel, Germany[a]
[18] Institute of Experimental Physics, Slovak Academy of Sciences, Košice, Slovak Republic[f,j]
[19] School of Physics and Chemistry, University of Lancaster, Lancaster, UK[b]
[20] Department of Physics, University of Liverpool, Liverpool, UK[b]
[21] Queen Mary and Westfield College, London, UK[b]
[22] Physics Department, University of Lund, Lund, Sweden[g]
[23] Physics Department, University of Manchester, Manchester, UK[b]
[24] CPPM, Université d'Aix-Marseille II, IN2P3-CNRS, Marseille, France
[25] Institute for Theoretical and Experimental Physics, Moscow, Russia
[26] Lebedev Physical Institute, Moscow, Russia[f]
[27] Max-Planck-Institut für Physik, München, Germany[a]
[28] LAL, Université de Paris-Sud, IN2P3-CNRS, Orsay, France
[29] LPNHE, Ecole Polytechnique, IN2P3-CNRS, Palaiseau, France
[30] LPNHE, Universités Paris VI and VII, IN2P3-CNRS, Paris, France
[31] Institute of Physics, Czech Academy of Sciences, Praha, Czech Republic[f,h]
[32] Nuclear Center, Charles University, Praha, Czech Republic[f,h]
[33] INFN Roma 1 and Dipartimento di Fisica, Università Roma 3, Roma, Italy
[34] Paul Scherrer Institut, Villigen, Switzerland
[35] Fachbereich Physik, Bergische Universität Gesamthochschule Wuppertal, Wuppertal, Germany[a]
[36] DESY, Institut für Hochenergiephysik, Zeuthen, Germany[a]
[37] Institut für Teilchenphysik, ETH, Zürich, Switzerland[i]
[38] Physik-Institut der Universität Zürich, Zürich, Switzerland[i]
[39] Institut für Physik, Humboldt-Universität, Berlin, Germany[a]
[40] Rechenzentrum, Bergische Universität Gesamthochschule Wuppertal, Wuppertal, Germany[a]
[41] Visitor from Physics Dept. University Louisville, USA

[a] Supported by the Bundesministerium für Bildung, Wissenschaft, Forschung und Technologie, FRG, under contract numbers 6AC17P, 6AC47P, 6DO57I, 6HH17P, 6HH27I, 6HD17I, 6HD27I, 6KI17P, 6MP17I, and 6WT87P
[b] Supported by the UK Particle Physics and Astronomy Research Council, and formerly by the UK Science and Engineering Research Council
[c] Supported by FNRS-NFWO, IISN-IIKW
[d] Partially supported by the Polish State Committee for Scientific Research, grant no. 115/E-343/SPUB/P03/120/96
[e] Supported in part by USDOE grant DE F603 91ER40674
[f] Supported by the Deutsche Forschungsgemeinschaft
[g] Supported by the Swedish Natural Science Research Council
[h] Supported by GA ČR grant no. 202/96/0214, GA AV ČR grant no. A1010619 and GA UK grant no. 177
[i] Supported by the Swiss National Science Foundation
[j] Supported by VEGA SR grant no. 2/1325/96

1 Introduction

The HERA collider allows the study of ep interactions over a wide range of squared four-momentum transfer, $-Q^2$, from photoproduction ($Q^2 \simeq 0$) to very high photon virtuality. This makes it possible to investigate the Q^2 dependence of particle production.

Photoproduction interactions are in many respects very similar to hadron-hadron interactions [1]. As Q^2 increases, the ep interaction is considered to be deep inelastic scattering (DIS) in which the exchanged virtual photon interacts directly with a parton in the proton.

The hadronic final state resulting from the fragmentation of partons is of a non-perturbative nature and is usually described using phenomenological models such as the string fragmentation scheme implemented in JETSET [2]. In contrast to the study of unidentified charged particles [3, 4], strange particles allow tagging of a specific quark species. Strange quarks are mainly produced in the hadronization phase, which is dominated by particles with low transverse momentum, p_t. However, they can also originate from hard partonic radiation and the direct interaction of a photon with the proton, e.g. boson-gluon fusion, thus contributing to the high-p_t tail of strange particles.

In this paper, the transverse momentum and rapidity spectra of K^0 and Λ particles in photoproduction at an average center of mass energy $\langle W \rangle = 200$ GeV are presented. These measurements are made in the photon fragmentation region, $1.3 < y^* < 2.8$, and the transverse momentum range $0.5 < p_t < 5$ GeV and are compared with results obtained in DIS at $\langle Q^2 \rangle = 23$ GeV^2 and a similar average W. The comparison is extended to the rapidity spectrum of charged particles to see if the similarities observed for strange particles are of a more general nature. This allows the investigation of the Q^2 dependence of particle production rates in the photon fragmentation region. In the central rapidity region these rates are generally assumed to be independent of Q^2 [5]. The process dependence of particle production rates is studied by comparing the rates of strangeness production in γp and in $p\bar{p}$. Finally, results from next-to-leading order (NLO) QCD calculations [6] and from PYTHIA [7, 2] are compared with the measurements.

2 Models of Photoproduction

The PYTHIA 5.7 Monte Carlo program, as used here, generates events according to the description given in [7, 2]. The structure of the photon is parameterized according to [7, 8]. Furthermore, the PYTHIA option of generating multiple interactions within the same event is used [9]. Fragmentation is performed using the Lund string fragmentation scheme, as implemented in JETSET 7.4. Matrix elements are calculated to leading order, and higher order terms are simulated by parton showers in the leading log approximation. The production rate of strange particles in JETSET is mainly controlled by the strangeness suppression factor, λ_s, that is, the probability of producing a strange quark pair relative to a light quark pair. By default λ_s is set to 0.3. However, recent deep inelastic muon nucleon scattering data from E665 [10], e^+e^- data from DELPHI [11] and ep data from H1 [12] and ZEUS [29] are better described by JETSET if $\lambda_s \simeq 0.2$ [1].

The authors of [6] calculate the inclusive single-particle photoproduction cross sections as follows. The hard subprocess is calculated to next-to-leading order in QCD, as is the evolution

[1] The following JETSET hadronization parameters have been changed with respect to the default settings (default/DELPHI/E665): Parj(2)=λ_s=(0.3/0.23/0.2), Parj(11)=(0.5/0.365/0.5), Parj(12)=(0.6/0.41/0.6). Parj(2) is the strangeness suppression factor, Parj(11) is the probability that a meson containing u or d quarks has spin 1, Parj(12) the probability that a meson containing s quarks has spin 1.

of the fragmentation and parton distribution functions. The fragmentation functions are derived from e^+e^- collider data. The parton distributions for the photon and the proton constitute an important input to the cross-section calculations. The numerical calculations presented here are based on the GRV parameterizations given in [13].

3 Experimental Procedure

3.1 Detector

The results presented in this paper are based on data taken in 1994 with the H1 detector. During this running period 820 GeV protons and 27.5 GeV positrons were brought into collision in HERA.

A full description of the H1 detector can be found in [14]. In this paper only the components of relevance to the measurements presented here are mentioned. These are the positron tagger, the central tracker, the backward proportional chamber (BPC), the backward electromagnetic calorimeter (BEMC) and the liquid argon (LAr) calorimeter. The direction of the z-axis is chosen to be along the proton beam direction. The polar angle θ is defined with respect to the z-axis and the pseudorapidity is given by $\eta = -\ln(\tan\theta/2)$.

The positron tagger, located 33 m from the interaction point in the positron direction, measures the energy of the scattered positron and, in conjunction with a photon detector, the luminosity by exploiting the Bethe-Heitler process [15].

The central track detector consists of an inner ($20 < R < 45$ cm) and an outer ($53 < R < 85$ cm) concentric central jet chamber (CJC), multi-wire proportional chambers for triggering purposes and two additional drift chambers which measure accurately the z-coordinate. The pseudorapidity range covered by the central track detector is $|\eta| < 1.5$.

The LAr calorimeter, which surrounds the tracking system, consists of an electromagnetic and a hadronic section. Here it is only used to identify and reject events containing a large rapidity gap in the forward direction, in the range $2.03 < \eta < 3.26$.

In the backward direction the BPC is used to determine the polar angle and the BEMC the energy of the scattered positron in DIS events. The pseudorapidity range covered by these detectors is $-3.35 < \eta < -1.51$.

The calorimeters are surrounded by a superconducting coil providing a uniform magnetic field of 1.15 T in the region occupied by the central tracker.

3.2 Event Selection

Photoproduction events are selected by requiring the presence of a scattered positron in the small angle positron tagger. For these events $Q^2 < 10^{-2}$ GeV ^{2}. The inelasticity of the scattering is given by $y = 1 - \frac{E'_e}{E_e} \cdot \sin^2\theta/2$. Here, E_e is the energy of the incident positron, E'_e and θ the energy and the polar angle of the scattered positron. In photoproduction, to a very good approximation, the inelasticity is given by $y = 1 - \frac{E'_e}{E_e}$. Photoproduction events are required to lie in the range $0.3 < y < 0.7$, in order to confine the scattered positron to a region in which the acceptance of the positron tagger is well understood. The trigger for these events requires a signal in the positron tagger and the presence of at least one negative track in the CJC. More information on this track-based trigger can be found in [16].

The trigger and the event selection for the DIS sample are as described in [12] except that the y range is restricted to ensure that the mean hadronic center of mass energies of the DIS and photoproduction samples are similar. The scattered positron is detected in the BEMC and is required to have an energy greater than 12 GeV and a polar angle between 150° and 173°. The kinematic variables are determined using the measured energy and angle of the scattered positron. The DIS sample is restricted to and corrected in the kinematic region given by $10 \leq Q^2 \leq 70$ GeV^2, $10^{-4} \leq x \leq 10^{-2}$ and $0.3 \leq y \leq 0.6$, where x is the Bjorken scaling variable.

For both the γp and DIS samples, the corresponding integrated luminosity is 1.3 pb^{-1}.

In addition to the measurements of strangeness production in γp and DIS, results on charged-particle production in these two processes are presented. For this purpose, a charged-particle photoproduction sample is selected consisting of events triggered by the coincident detection of a positron in the small angle positron tagger and at least one track pointing to the interaction vertex with $p_t > 200$ MeV measured in the cylindrical multi-wire proportional chambers. The charged-particle DIS sample consists of events which are triggered by a cluster in the BEMC with an energy deposit of more than 4 GeV. For both the DIS and γp charged-particle samples, the inelasticity y of the interaction is restricted to $0.3 < y < 0.5$, resulting in an average W of 187 GeV. The DIS sample is restricted to the range $8 < Q^2 < 30$ GeV^2 giving an average $\langle Q^2 \rangle = 15$ GeV^2. The charged-particle data samples studied correspond to an integrated luminosity of 1.5 pb^{-1}.

Common to all four event samples is the requirement of a reconstructed primary vertex within 30 cm of the nominal vertex position.

The background from photoproduction in the two DIS data samples is estimated to be less than 3%.

For a comparison of particle production in different processes it is important to take into account the different contributions of low-mass diffractive events. While in the case of DIS this fraction is only 10%, it is around 30% in photoproduction [17, 18]. These events are characterized by the absence of energy deposited in the forward direction. To allow a direct comparison between DIS and γp these large rapidity gap events are removed from the samples by requiring the presence of at least 500 MeV of energy in the forward region of the liquid argon calorimeter, $2.03 < \eta < 3.26$. The remaining samples are termed non-diffractive in the following.

3.3 K^0_S and Λ Identification in Photoproduction

K^0_S mesons and Λ baryons are identified through their decay channels

$$K^0_S \to \pi^+\pi^-$$

$$\Lambda(\bar{\Lambda}) \to p\pi^-(\bar{p}\pi^+)$$

where the pion, the proton and the antiproton tracks are reconstructed in the CJC. The tracks of the decay products are required to satisfy $|\eta| < 1.5$ and $p_t > 180$ MeV, where p_t is defined with respect to the beam axis. This restricts the acceptance to a region where the reconstruction efficiency is high. In addition, it is required that the radial positions r_{beg} and r_{end} of the first and last measured point on the tracks fulfill $r_{beg} < 30$ cm and $r_{end} > 37.5$ cm and that their radial length be at least 10 cm. Candidates for neutral particles decaying into two charged particles, hereafter called V^0 candidates, are searched for by performing a constrained fit to each pair of oppositely charged tracks. The fit demands that the tracks meet at a common secondary vertex and that the two particle momenta of the decay products transverse to the path of flight of the

V^0 candidate be opposite. The V^0 candidate invariant masses are calculated assuming that the decay products are two pions for K^0_S candidates and a proton and a pion for Λ candidates.

To reduce the combinatorial background and ensure good reconstruction of the decay, the radial distance d_r from the primary to the secondary vertex is restricted to $2 < d_r < 18$ cm for the K^0_S and $3 < d_r < 18$ cm for the Λ candidates. Note that Λ decays with $d_r < 3$ cm have a lower reconstruction probability due to the large asymmetry in the p_t of the decay particles.

The contamination from Λ decays in the K^0_S sample is reduced to a negligible level by demanding that the transverse momentum of the decay particles with respect to the momentum of the V^0 candidate be greater than 120 MeV. Likewise, the K^0_S contamination in the Λ sample is removed by excluding those Λ candidates for which the $\pi^+\pi^-$ invariant mass, $m_{\pi\pi}$, falls in the window $0.48 < m_{\pi\pi} < 0.52$ GeV.

The applied cuts ensure that kinematic regions in which the reconstruction efficiencies for K^0_S and Λ start to degrade are avoided. The large number of K^0_S candidates makes it possible to exclude in addition regions in azimuth, φ, of the CJC which have known imperfections (and where systematic effects are larger) and to reject K^0_S topologies which are dominated by combinatorial background [19].

In order to ensure an optimal acceptance of the CJC for the V^0's, their pseudorapidity has been restricted to $|\eta| < 1.3$ and their transverse momentum to $0.5 < p_t < 5$ GeV for K^0_S and to $0.6 < p_t < 5$ GeV for Λ.

The final K^0_S and Λ signals, after applying all the aforementioned cuts, are shown in Fig. 1. Approximately 7 700 K^0_S candidates and 3 600 Λ candidates remain. In the fits the signals are described by a superposition of two gaussians on a linear background, accounting for varying invariant mass resolutions for different decay topologies. On average the RMS width of the K^0_S signal is 9.2 MeV, the RMS width of the Λ signal is 2.9 MeV. The fitted peak positions are in agreement with the PDG K^0 and Λ masses [20] within the systematic errors resulting from performing the above fits using various functional forms and from remaining uncertainties in the calibration of the tracking system.

3.4 Corrections and Systematic Errors

In order to obtain the inclusive K^0 and Λ photoproduction cross sections it is necessary to correct the observed numbers of K^0_S mesons and Λ baryons for the branching ratios into the observed decay channels, and for the acceptances and efficiencies of the various detector components.

The dependence of the acceptance of the positron tagger on the inelasticity, y, is known from a measurement of the tagger acceptance for the Bethe-Heitler process $ep \to ep\gamma$ and Monte Carlo studies of the luminosity system and the HERA beam optics. More details can be found in [21].

The efficiency of the track trigger is studied by using a reference event sample obtained with an independent trigger which does not make any requirement on the hadronic final state. On average it is found to be 85% and only weakly dependent on the transverse momentum of the V^0. The systematic uncertainty associated with the trigger efficiency is less than 6%. This has been cross-checked by using a sample of simulated and reconstructed events.

A visual check of the efficiency for reconstructing tracks satisfying the requirements described in the previous section reveals that it is consistent with the estimate of 98% obtained in [22]. The systematic uncertainty assigned to this correction factor is 2%.

The main correction results from the limited geometric acceptance of the CJC for V^0 decays and the cuts applied to select V^0 candidates explained in the previous section. The acceptance

can be parameterized as a function of the p_t and η of the V^0 and ranges between 3% and 17% for K^0_S and between 4% and 25% for Λ decays. The cuts which have a large effect on the acceptance are the lower cuts on d_r and p_t of the decay tracks and, in the case of the K^0_S, the φ cut. The bin-dependent systematic uncertainty on the acceptance calculation is estimated by varying all cuts independently and re-evaluating the cross section. In a given bin the maximum variation is taken as a measure of the systematic error resulting from the acceptance correction. The bin-dependent systematic errors are listed in Tab. 1 and 2 and range between 2% and 10%.

Within the region defined by the above cuts the efficiency for reconstructing V^0's is found to be 100% using a full detector simulation of photoproduction events. Since the K^0 analysis is restricted to the fully efficient regions of the CJC, which are well simulated, no additional correction is applied. For the reconstruction of Λ decays a detection efficiency of 97% is found. This leads to a systematic error of $^{+2}_{-0}$% for K^0_S and $^{+5}_{-3}$% for Λ.

The background resulting from non-ep interactions (proton wall and proton gas interactions) has been estimated from the proton pilot-bunch events, that is, events where the proton bunch does not have a colliding positron bunch partner. This background has been found to be negligible, but a systematic uncertainty of $^{+0}_{-2}$% is assigned to its contribution to the cross section.

The systematic uncertainty of the luminosity determination is 1.5% [23].

The overall bin-independent systematic error is calculated by adding the various contributions in quadrature and results in errors of ± 8% for the K^0 cross section and $^{+9}_{-8}$% for the Λ cross section.

For the charged-particle spectra, the dominant contributions to the systematic error, both in photoproduction and DIS, originate from the extrapolation to $p_t = 0$ (5%). The extrapolation was performed using a sample of fully simulated Monte Carlo events. The resulting error was estimated by varying the minimum p_t of the particles both in Monte Carlo and data. In the case of the total charged-particle photoproduction sample an additional uncertainty in the losses of events with low charged-particle multiplicity (6%) is taken into account.

4 Experimental Results

Comparisons between the photoproduction data and the above-mentioned models and calculations are performed in the laboratory frame. Comparisons of strangeness production in photoproduction with that in DIS and $p\bar{p}$ interactions are made in the photon-proton and the proton-antiproton center of mass systems, using the non-diffractive data sample. The transverse momentum, p_t, and the rapidity, y^*, are defined with respect to the direction of the exchanged boson for DIS and with respect to the direction of the positron beam for γp. In the case of $p\bar{p}$, p_t and $|y^*|$ are defined with respect to the beam axis.

In Tab. 1 and 2 the total γp cross sections for K^0, Λ and $\bar{\Lambda}$ production are presented as a function of p_t and rapidity y^*. The y^* range has been restricted to $1.3 < y^* < 2.8$ to make the measurement insensitive to the θ acceptance of the CJC. The p_t spectra fall steeply whereas there is almost no dependence on y^* in the measured rapidity interval.

Here and in what follows, all K^0_S results are multiplied by 2 and therefore correspond to K^0 and $\bar{K^0}$ production; no distinction is made between K^0 and $\bar{K^0}$ and the combination of both is denoted by K^0. Furthermore, it can be seen that the Λ cross section is, within errors, equal to the $\bar{\Lambda}$ cross section. Therefore they are combined and subsequent references to Λ always mean $\Lambda + \bar{\Lambda}$.

For photoproduction the $ep \to V^0X$ cross section σ_{ep} is related to the $\gamma p \to V^0X$ cross section $\sigma_{\gamma p}(W)$ by the Weizsäcker-Williams formula [24]

$$\sigma_{ep} = \sigma_{\gamma p}(W) \cdot F$$

where $F = 0.0136$ is the flux factor integrated over $0.3 < y < 0.7$ and $Q^2 < 10^{-2}$ GeV^2.

	p_t range [GeV]		$\frac{1}{\Delta y^*}\frac{d\sigma}{dp_t^2}$ [nb/GeV^2]	stat.	syst.
a) K^0:	0.5	0.6	25500	1400	500
	0.6	0.7	16700	900	300
	0.7	0.8	11300	600	200
	0.8	0.9	7800	400	300
	0.9	1.0	4900	300	200
	1.0	1.2	3200	100	200
	1.2	1.4	1600	100	50
	1.4	1.8	570	30	30
	1.8	2.2	190	20	10
	2.2	3.0	38	5	3
	3.0	5.0	3.6	0.9	0.4
b) Λ:	0.6	0.9	1900	100	100
	0.9	1.2	630	30	40
	1.2	1.7	190	10	20
	1.7	3.0	17	2	1
c) $\overline{\Lambda}$:	0.6	0.9	1700	100	100
	0.9	1.2	600	30	30
	1.2	1.7	200	10	20
	1.7	3.0	15	2	1

Table 1: Inclusive K^0 (a) and $\Lambda/\overline{\Lambda}$ (b,c) total γp production cross sections $1/\Delta y^* \cdot d\sigma/dp_t^2$ for $1.3 < y^* < 2.8$. The systematic errors given in the table do not include an overall systematic uncertainty of $\pm 8\%$ for K^0 and $^{+9}_{-8}\%$ for Λ as explained in section 3.4.

4.1 Comparison with Models and Calculations

In this section the predictions of PYTHIA in combination with JETSET, and the results of next-to-leading order calculations, are confronted with the measurements reported in this paper.

Figure 2 shows a comparison of the measured K^0 and Λ cross sections in p_t and η with the predictions of PYTHIA using standard parameter settings ($\lambda_s = 0.3$) as well as parameter sets obtained from fits to DELPHI and E665 data, as described in section 2. In the case of K^0 mesons (Fig. 2 a,b) the measured cross sections are in reasonable agreement with the Monte Carlo predictions using the DELPHI or E665 settings whereas the predictions with the standard settings seem to overestimate the cross section. However, the measured Λ (Fig. 2 c,d) cross section lies significantly above the Monte Carlo prediction for all three scenarios. The UA5 collaboration has reported a similar discrepancy between Λ production in $p\bar{p}$ interactions at 200 GeV and PYTHIA predictions [25]. No attempt is made here to tune the JETSET parameters controlling diquark production.

	y^* range		$\frac{d\sigma}{dy^*}$ [nb]	stat.	syst.
a) K^0:	1.30	1.55	13500	600	700
	1.55	1.80	12700	600	400
	1.80	2.05	13200	600	300
	2.05	2.30	11800	600	500
	2.30	2.55	12600	600	400
	2.55	2.80	12200	600	400
b) Λ:	1.300	1.675	1900	100	100
	1.675	2.050	1600	100	100
	2.050	2.425	1600	100	300
	2.425	2.800	1500	100	100
c) $\overline{\Lambda}$:	1.300	1.675	1900	100	100
	1.675	2.050	1600	100	100
	2.050	2.425	1300	100	200
	2.425	2.800	1400	100	100

Table 2: Inclusive K^0 (a) and $\Lambda/\overline{\Lambda}$ (b,c) total γp production cross sections $d\sigma/dy^*$ for $0.5 < p_t < 5$ GeV in the case of K^0's and $0.6 < p_t < 5$ GeV in the case of Λ's. The systematic errors given in the table do not include an overall systematic uncertainty of $\pm 8\%$ for K^0 and $^{+9}_{-8}\%$ for Λ as explained in section 3.4.

Recent next-to-leading order QCD calculations of inclusive particle spectra in ep scattering use fragmentation functions which have been fitted to e^+e^- data [6]. These NLO calculations involve four scales: the factorization scales connected with the parton densities of the photon and the proton, the factorization scale of the fragmentation functions and the renormalization scale of the QCD coupling constant. The calculations for K^0 cross sections assume that all four scales are equal; they are taken to be equal to $p_t/2$, p_t or $2p_t$ (where p_t is the transverse momentum of the K^0). This arbitrariness in the choice of the scales introduces a change in the predicted cross sections and is a measure of the contribution of higher-order terms. To reduce the scale influence, the calculation for the photoproduction of neutral kaons was restricted to transverse K^0 momenta $p_t > 1$ GeV, although the theoretical predictions should be more reliable for transverse momenta above 3 GeV [6]. A comparison of data with this calculation is shown in Fig. 3. In the high p_t region the agreement is satisfactory. Below 2 GeV the calculation deviates significantly from the data.

4.2 Comparison to Deep Inelastic Scattering and $p\bar{p}$

A comparison of K^0 production rates in γp and DIS is shown in Fig. 4 and a similar comparison of Λ production rates in Fig. 5 for the non-diffractive event samples defined in section 3.2. The γp and DIS rates are compatible in y^* and at low p_t. At high p_t, where possible differences in the underlying hard subprocesses may manifest themselves (charm production via photon-gluon fusion, hard gluon radiation in DIS, resolved photon contribution in γp), the DIS data lie somewhat above the γp data.

It is of interest to investigate if such an agreement in rates extends to other processes, such as, for instance, $p\bar{p}$ collisions. Figure 6 shows a comparison of K^0 and Λ production in $p\bar{p}$ collisions at 200 GeV, obtained by the UA5 collaboration and the present photoproduction measurement.

The UA5 K^0_S data [26] have been multiplied by 2 to convert the K^0_S rates to K^0 and $\bar{K^0}$ rates, and divided by the width of the rapidity range in which the measurement has been performed ($|y^*| < 2.5$). In the case of the UA5 Λ data [25] the rapidity range is restricted to $|y^*| < 2$. The trigger of the UA5 experiment rejected events in which either only the p or $\bar{p}$ dissociate, as well as elastic events. This sample, termed non-single diffractive, may be compared to the non-diffractive samples of the present measurement as low-mass diffractive events are removed in both cases. It can be seen that the K^0 production rates (Fig. 6a) are in good agreement. In contrast, the Λ rates in the photon fragmentation region in photoproduction are lower than in $p\bar{p}$ interactions. This may be attributable to the presence of an initial baryon in $p\bar{p}$ in this hemisphere from the incoming proton or antiproton. A difference between photon and target fragmentation region with respect to baryon production has also been observed in deep inelastic μN scattering [10].

Given the observed process independence of the low p_t K^0 meson production rates, it may be asked if such a feature holds for other mesons. In order to answer this question, the rate of production of charged particles, which consist mostly of charged pions and kaons, was investigated in γp and DIS.

For this analysis the charged particles are accepted in the extended rapidity range $0.5 < y^* < 3.5$. At the limits of this range the geometric acceptance decreases to 80%.

Figure 7 shows the comparison of charged-particle rates observed in DIS and γp. Here the data are extrapolated to $p_t = 0$ using samples of Monte Carlo events which include a full simulation of the effects of the H1 detector. In Fig. 7a, where all events contribute to the center of mass rapidity spectrum, it can be seen that the rate in DIS is significantly higher than in γp. When the (low mass) diffractive events are removed (Fig. 7b), the rates are comparable in both samples within errors.

The simple quark parton model does not predict an explicit Q^2 dependence of the particle production rates but it can be argued that perturbative QCD would introduce such a dependence [27]. A small Q^2 dependence was reported by EMC [28] for charged particles, but this dependence decreases with increasing W.

The present measurement does not indicate a significant change of non-diffractive production rates for K^0, Λ and charged particles in the photon fragmentation region when Q^2 changes from $Q^2 \simeq 0$ to $Q^2 \simeq 20$ GeV^2. This extends the observations made at higher Q^2 by H1 for charged particles [3] and by ZEUS for strange particles [29] that there is little or no dependence of the average particle multiplicities on Q^2. However, it should be kept in mind that the spectra investigated here are dominated by low p_t particles. At higher p_t, as mentioned earlier, the DIS and γp kaon rates show a small discrepancy. This observation is consistent with results published by H1 showing that for $p_t > 1$ GeV the charged-particle rates increase with increasing Q^2 [4].

5 Conclusion

The K^0 and Λ production cross sections have been measured in photoproduction and DIS with the H1 detector at HERA, at an average γp center of mass energy of about 200 GeV, as a function of the transverse momentum and the rapidity, in a kinematic range corresponding to the photon fragmentation region. No significant enhancement of the non-diffractive K^0 and Λ production rates is observed when going from $Q^2 \simeq 0$ to $Q^2 \simeq 20$ GeV^2. This feature has been found to hold also for the charged-particle non-diffractive production rates. At higher p_t, however, the K^0 rate in DIS is somewhat higher than in γp. The K^0 rate has been found to be similar to that measured in $p\bar{p}$ interactions at the same center of mass energy. However the

measured Λ rate is lower than in $p\bar{p}$. The measured K^0 spectra have been found to be broadly consistent with PYTHIA and NLO predictions, whereas the measured Λ spectra are significantly underestimated by PYTHIA.

Acknowledgments

We are grateful to the HERA machine group whose outstanding effort made this experiment possible. We appreciate the immense effort of the engineers and technicians who built and maintained the detector. We thank the funding agencies for financial support. We acknowledge the support of the DESY technical staff. We wish to thank the DESY directorate for the hospitality extended to the non-DESY members of the collaboration. We also want to thank J. Binnewies, B.A. Kniehl and G. Kramer for fruitful discussions and making the results of their calculations available to us.

References

[1] T.H. Bauer, R.D. Spital, D.R. Yennie, F.M. Pipkin, *Rev. Mod. Phys.* **50**, (1978) 261; ERRATUM *ibid.* **51**, (1979) 407.

[2] T. Sjöstrand, *Comp. Phys. Comm.* **82** (1994) 74.

[3] H1 Coll., S. Aïd et al., *Z. Phys.* **C72** (1996) 573.

[4] H1 Coll., S. Aïd et al., *Nucl. Phys.* **B485** (1997) 3.

[5] J.D. Bjorken, J. Kogut, *Phys. Rev.* **D8** (1973) 1341.

[6] J. Binnewies, B.A. Kniehl, G. Kramer, *Phys. Rev.* **D53**, (1996) 3573.

[7] G.A. Schuler, T. Sjöstrand, *Nucl. Phys.* **B407** (1993) 539.

[8] W. Glück. E. Reya, A. Vogt, *Z. Phys.* **C53** (1991) 651.

[9] H1 Coll., S. Aïd et al., *Z. Phys.* **C70** (1996) 17.

[10] E665 Coll., M.R. Adams et al., *Z. Phys.* **C61** (1994) 539.

[11] DELPHI Coll., P. Abreu et al., *Z. Phys.* **C65** (1995) 587.

[12] H1 Coll., S. Aïd et al., *Nucl. Phys.* **B480** (1996) 3.

[13] W. Glück. E. Reya, A. Vogt, *Phys. Rev.* **D46** (1992) 1973.

[14] H1 Coll., I. Abt et al., *Nucl. Instr. and Meth.* **A386** (1997) 310; *ibid.* **A386** (1997) 348.

[15] H1 Coll., I. Abt et al., *Z. Phys.* **C66** (1995) 529.

[16] J. Riedlberger, The H1 Trigger with emphasis on Tracking Triggers, contr. paper to 5th International Conference on Advanced Technology and Physics, Como 1994.

[17] H1 Coll., T. Ahmed et al., *Nucl. Phys.* **B435** (1995) 3.

[18] H1 Coll., T. Ahmed et al., *Nucl. Phys.* **B429** (1994) 477.

[19] K. Johannsen, Ph.D. thesis, Universität Hamburg, DESY FH1-96-01, (1996), unpublished.

[20] R.M. Barnett et al., Particle Data Group, **D54** (1996) 412.

[21] H1 Coll., S. Aïd et al., *Z. Phys.* **C69** (1995) 27.

[22] W. Erdmann, Ph.D. thesis, ETH Zürich, No. 11441, (1996), unpublished.

[23] S. Aïd et al., *Nucl. Phys.* **B470** (1996) 3.

[24] C.F. Weizsäcker, *Z. Phys.* **88** (1934) 612;
E.J. Williams, *Phys. Rev.* **45** (1934) 729;
S. Frixione et al., *Phys. Lett.* **B319** (1993) 339.

[25] UA5 Coll., R.E. Ansorge et al., *Nucl. Phys.* **B328** (1989) 36.

[26] UA5 Coll., R.E. Ansorge et al., *Z. Phys.* **C41** (1988) 179.

[27] Yu.L. Dokshitzer, V.A. Khoze, A.H. Mueller, S.I. Troyan, Basics of perturbative QCD, *Ed. Frontieres* (1991).

[28] EMC Coll., M. Arneodo et al., *Z. Phys.* **C31** (1986) 1.

[29] ZEUS Coll., M. Derrick et al., *Z. Phys.* **C68** (1995) 29.

6 Figures

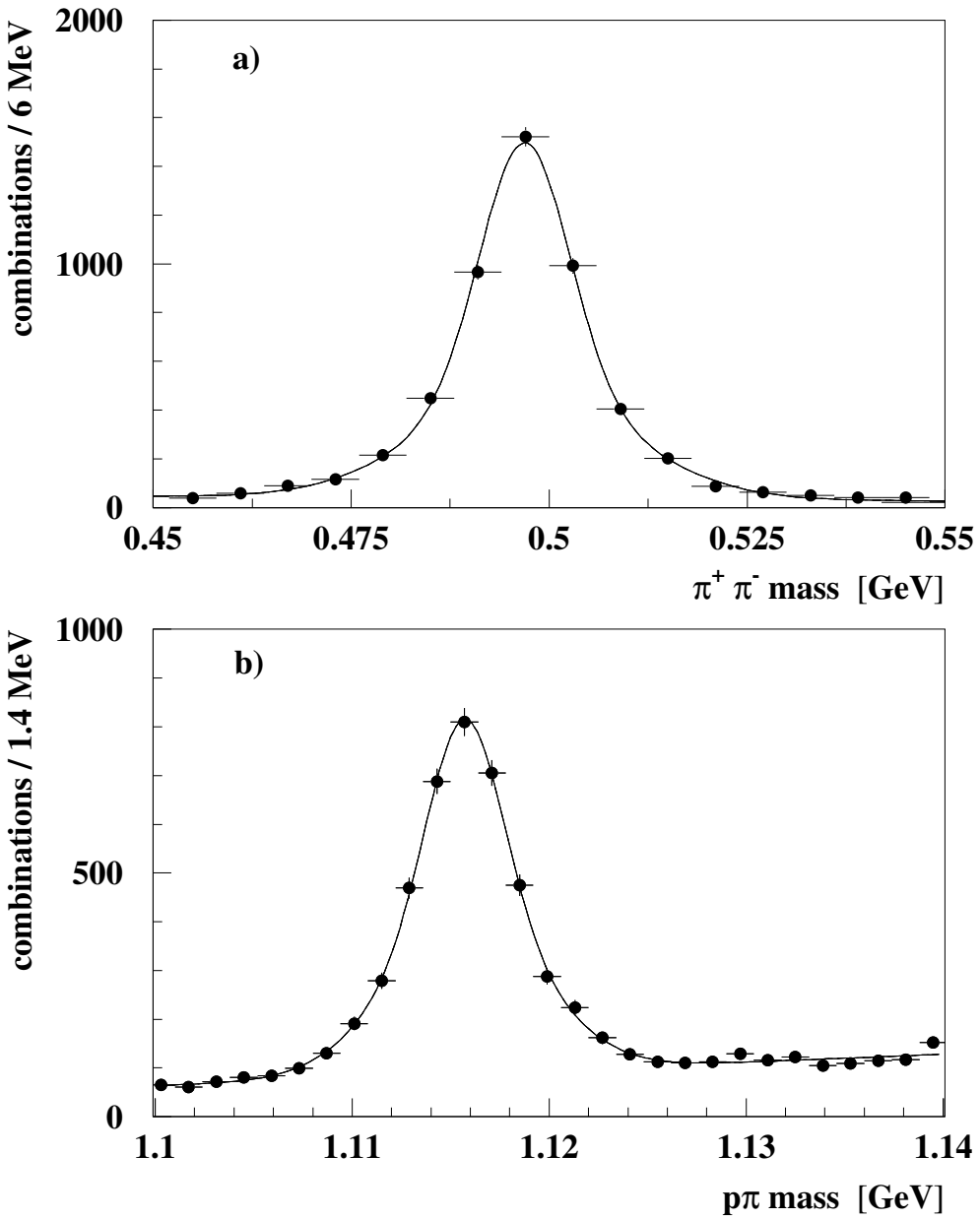

Figure 1: Invariant mass distributions for K^0_S (a) and Λ (b) candidates in photoproduction, after applying all the cuts described in the text. The K^0_S candidates are restricted to the kinematic range $|\eta| < 1.3$ and $0.5 < p_t < 5$ GeV; the Λ candidates are restricted to the kinematic range $|\eta| < 1.3$ and $0.6 < p_t < 5$ GeV. The curves represent the fits as described in the text.

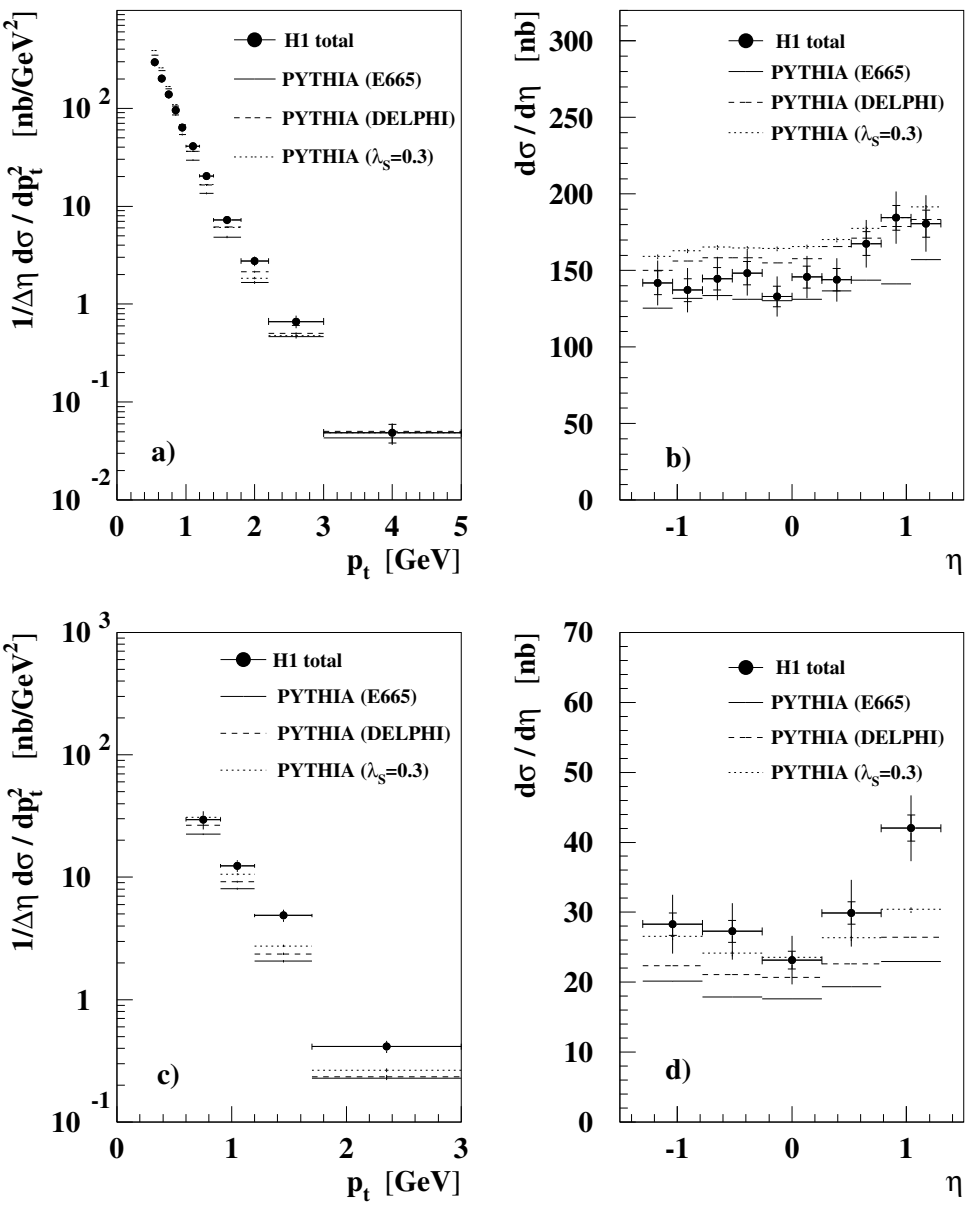

Figure 2: Measured K^0 (a,b) and Λ (c,d) total ep cross sections in photoproduction as a function of p_t and pseudorapidity η compared to PYTHIA in the kinematic range $|\eta| < 1.3$ and $0.5 < p_t < 5$ GeV. The inner vertical error bars indicate the statistical error only and the outer error bars the statistical and total systematic error added in quadrature. The labels E665 and DELPHI correspond to JETSET parameters favored by these experiments; the label $\lambda_s = 0.3$ denotes standard JETSET settings.

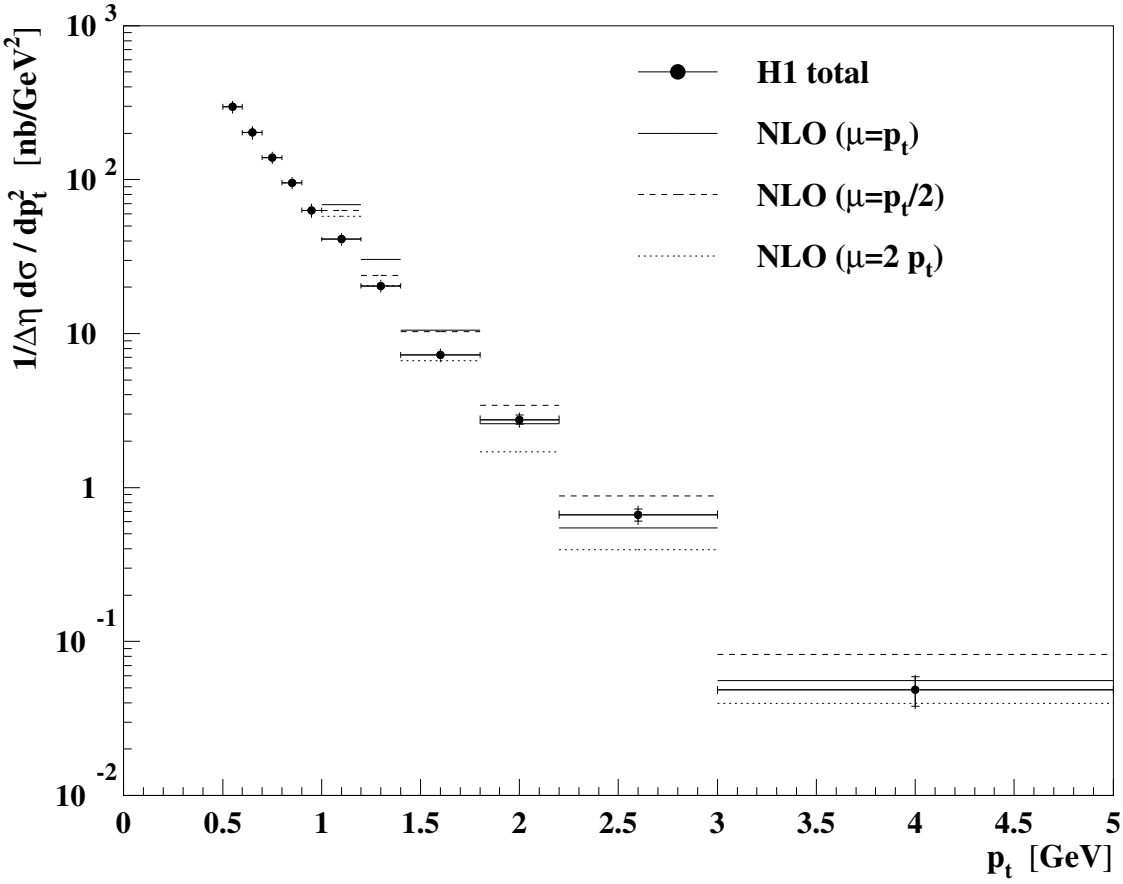

Figure 3: Measured K^0 total ep cross section in photoproduction as a function of p_t compared to NLO calculations in the kinematic range $|\eta| < 1.3$ and $0.5 < p_t < 5$ GeV. The inner vertical error bars indicate the statistical error only and the outer error bars the statistical and total systematic error added in quadrature. The NLO curves correspond to different values of the renormalization and factorization scales μ, namely p_t, $2p_t$ and $p_t/2$, where p_t is the transverse momentum of the K^0.

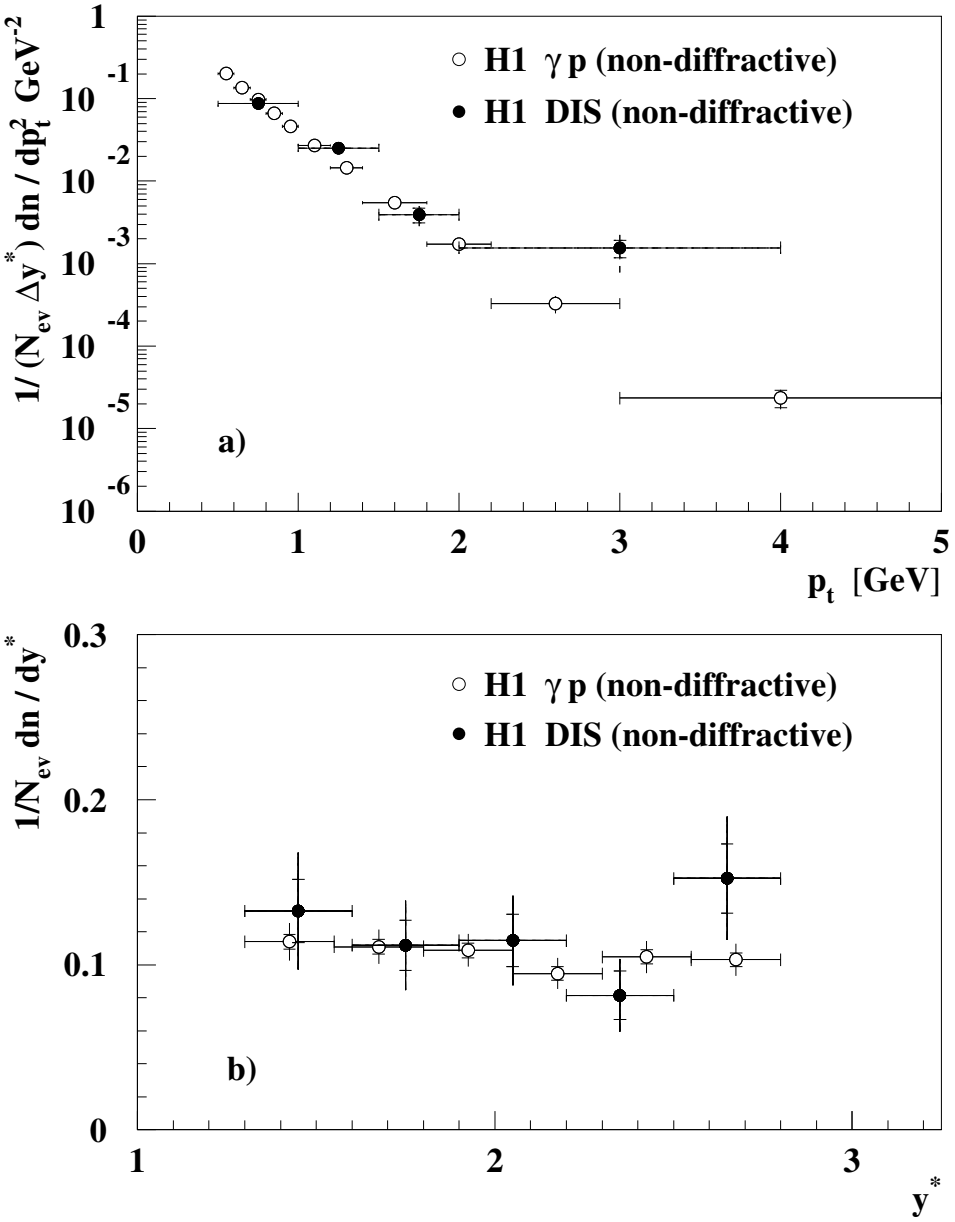

Figure 4: K^0 rate as a function of p_t (a) and center of mass rapidity y^* (b) in γp and DIS for non-diffractive events. The data are integrated over $1.3 < y^* < 2.8$ in (a), and over $p_t > 0.5$ GeV in (b). The inner vertical error bars indicate the statistical error only and the outer error bars the statistical and total systematic error added in quadrature.

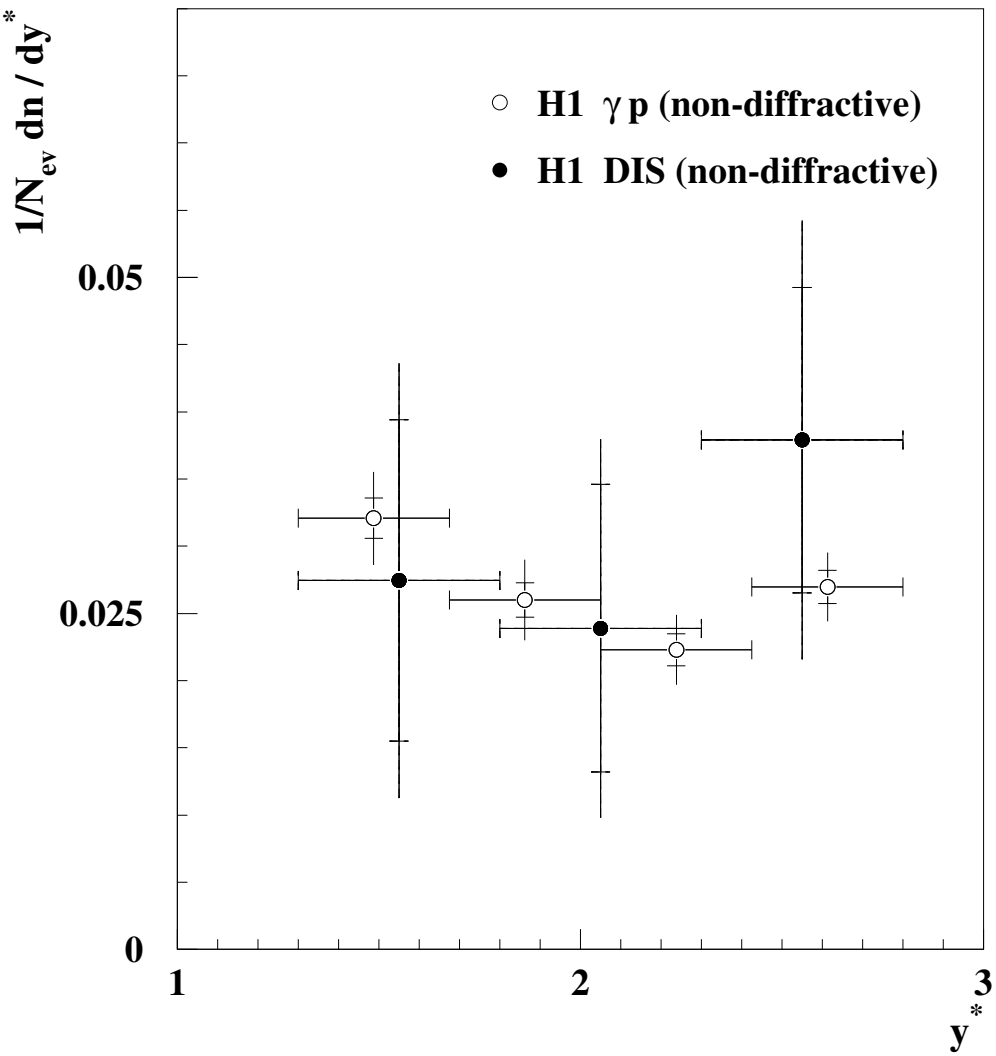

Figure 5: Λ rate as a function of center of mass rapidity y^* in γp and DIS for non-diffractive events. The data are integrated over $p_t > 0.6$ GeV. The inner vertical error bars indicate the statistical error only and the outer error bars the statistical and total systematic error added in quadrature.

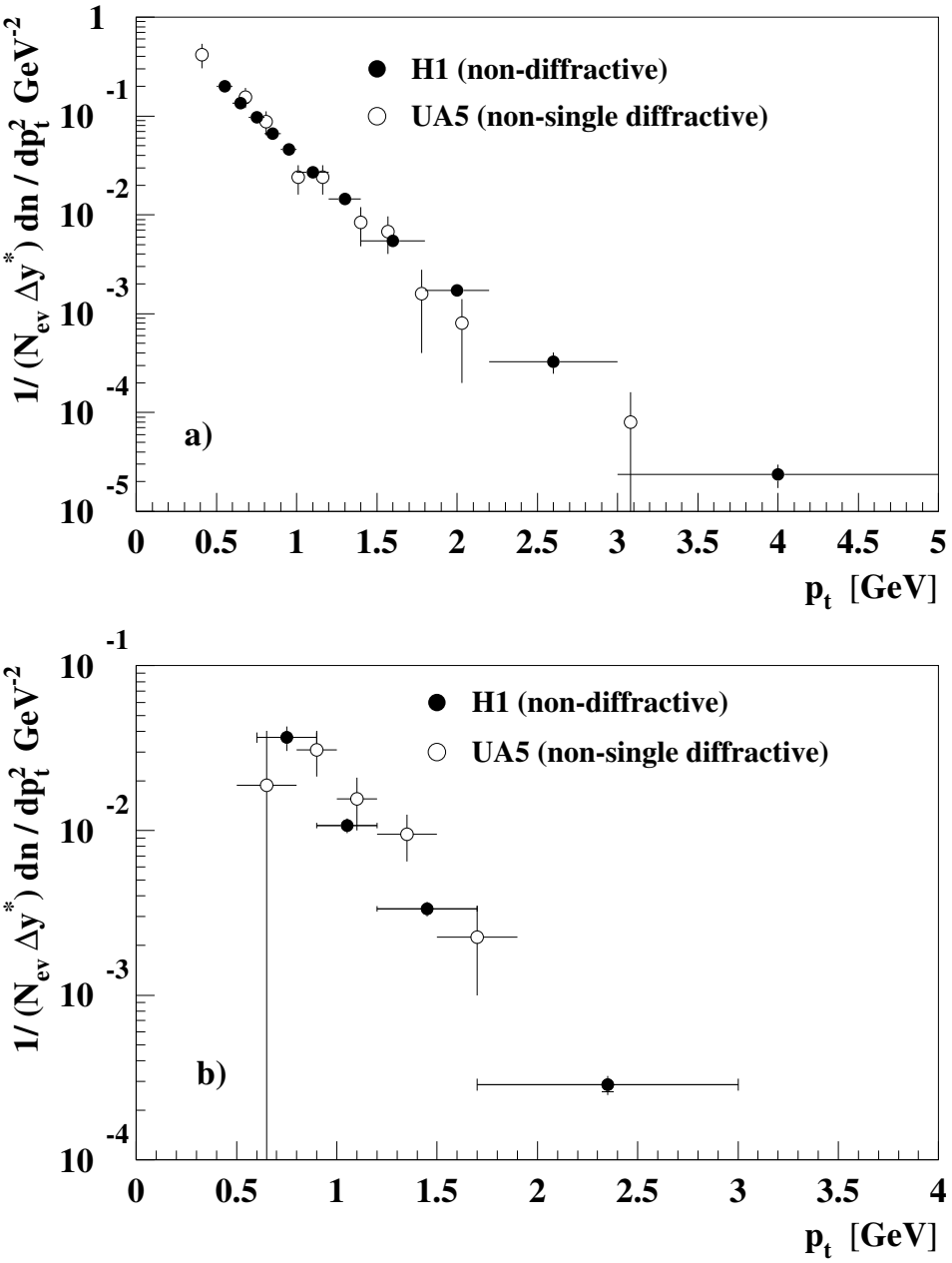

Figure 6: K^0 rate (a) and Λ rate (b) as a function of p_t in γp and $p\bar{p}$ (UA5) for non-diffractive events. The H1 data are integrated over $1.3 < y^* < 2.8$ and the UA5 data are normalized to the same rapidity range. The inner vertical error bars indicate the statistical error only and the outer error bars the statistical and total systematic error added in quadrature.

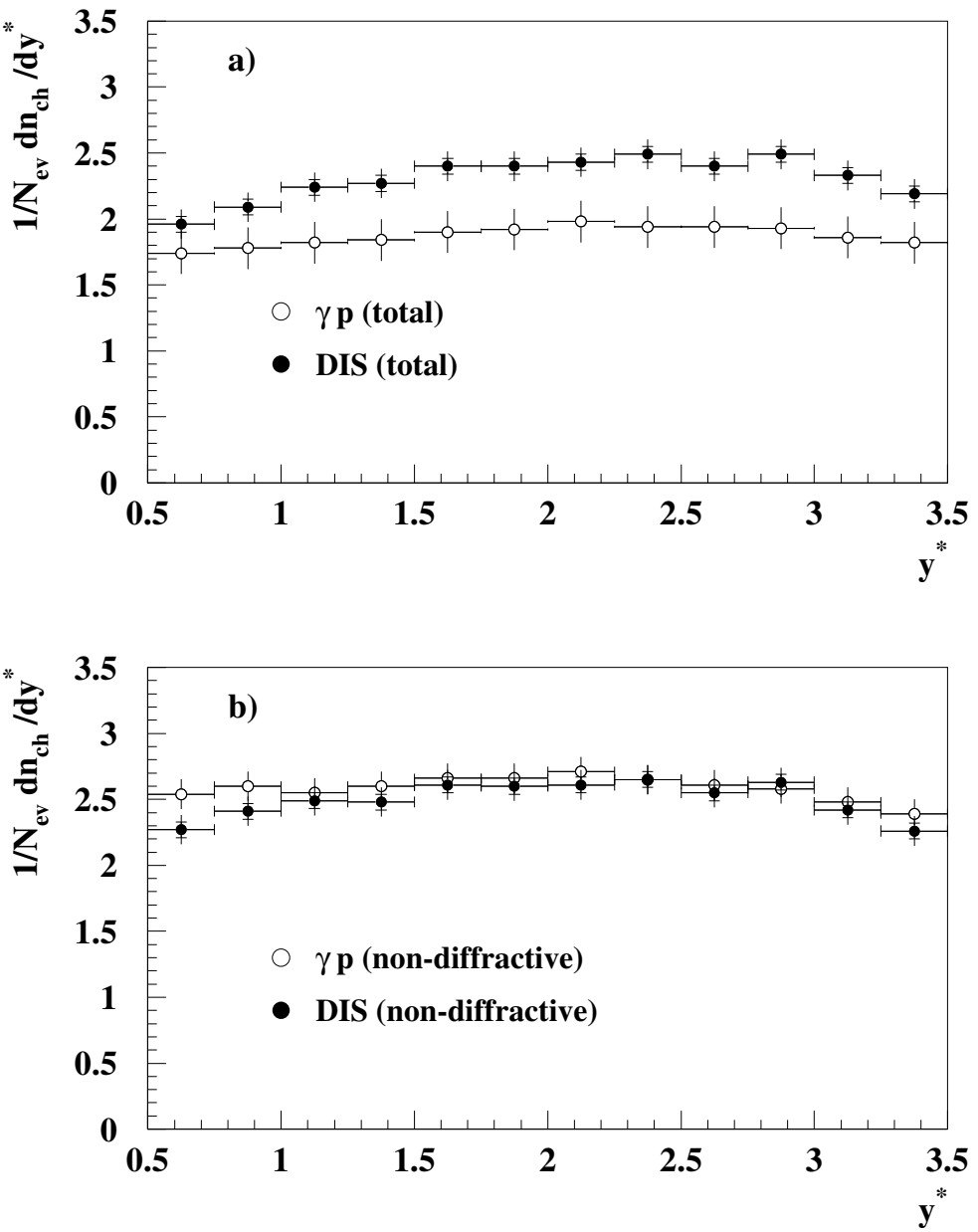

Figure 7: The charged-particle center of mass rapidity distribution in DIS and γp for all events (a) and non-diffractive events (b). The data have been extrapolated down to $p_t = 0$. The inner vertical error bars indicate the statistical error only and the outer error bars the statistical and total systematic error added in quadrature.